nature photonics

LETTERS

PUBLISHED ONLINE: 14 DECEMBER 2008 | DOI: 10.1038/NPHOTON.2008.251

Magnetic-field-assisted terahertz quantum cascade laser operating up to 225 K

A. Wade[1], G. Fedorov[1], D. Smirnov[1]*, S. Kumar[2], B. S. Williams[2,3], Q. Hu[2] and J. L. Reno[4]

Advances in semiconductor bandgap engineering have resulted in the recent development of the terahertz quantum cascade laser[1]. These compact optoelectronic devices now operate in the frequency range 1.2–5 THz, although cryogenic cooling is still required[2,3]. Further progress towards the realization of devices operating at higher temperatures and emitting at longer wavelengths (sub-terahertz quantum cascade lasers) is difficult because it requires maintaining a population inversion between closely spaced electronic sub-bands (1 THz ≈ 4 meV). Here, we demonstrate a magnetic-field-assisted quantum cascade laser based on the resonant-phonon design. By applying appropriate electrical bias and strong magnetic fields above 16 T, it is possible to achieve laser emission from a single device over a wide range of frequencies (0.68–3.33 THz). Owing to the suppression of inter-Landau-level non-radiative scattering, the device shows magnetic field assisted laser action at 1 THz at temperatures up to 215 K, and 3 THz lasing up to 225 K.

In quantum cascade lasers (QCLs), radiative transitions take place between size-quantized sub-bands within the conduction band of a multi-quantum well system. Quantum well thickness can therefore be varied, allowing the emission wavelength to be tailored, using the same material, to cover a broad range of frequencies. Since the first demonstration of a mid-infrared (MIR) QCL in 1994 (ref. 4), rapid progress has been made in QCL design and materials growth, with the result that QCLs have become the dominant MIR semiconductor laser source[5–7].

In a terahertz QCL, the photon emission energy is smaller than the longitudinal-optical (LO) phonon energy in the semiconductor material of the quantum well, $h\nu < \hbar\omega \approx 36$ meV (GaAs). In the resonant-phonon design scheme, the population inversion is ensured by selectively injecting electrons through resonant tunnelling into the upper state of the laser transition. Relaxation from the lower radiative state occurs on a subpicosecond timescale into the injector states through LO-phonon emission[8–10]. This scheme has the highest operation temperature of any terahertz QCL design to date ($T_{max} = 178$ K)[9,10].

Achieving high-temperature operation in terahertz QCLs is difficult, because although $h\nu < \eta\omega_{LO}$, as the temperature increases, electrons in the upper radiative state gain sufficient in-plane energy to emit an LO-phonon, which results in a fast thermally activated scattering process and a reduction in gain. The use of zero-dimensional confinement in quantum cascade structures has been proposed as a mechanism to suppress non-radiative intersub-band/level relaxation and achieve lower threshold and higher temperature operation[11–14]. Although appropriate technology does not exist at this time, a magnetic field is an effective tool to analyse and improve the performance of MIR[15,16] and terahertz[17–19] QCLs in the zero-dimensional limit. A magnetic field changes the two-dimensional parabolic energy dispersion of each size-quantized sub-band $\varepsilon_n(k)$ into a set of discrete, equidistant, zero-dimensional-like Landau levels (LLs), $\varepsilon_{n,N} = E_n + (N + 1/2)\hbar\omega_c$, separated by the cyclotron energy $\hbar\omega = \hbar eB/m^*$, where n is the sub-band index, N is the LL index, B is the magnetic field, and m^* is the energy-dependent electron effective mass. As a result, both radiative and non-radiative transitions are either reduced or resonantly enhanced by the inelastic (LO-phonon assisted[15]) or (quasi)-elastic (interface roughness, acoustical phonons or impurities[16]) scattering between different LL states $|n,N\rangle$. Here, we exploit this approach of 'Landau-level engineering' to explore the ultimate limits of terahertz QCL operation.

The samples used were GaAs/$Al_{0.15}Ga_{0.85}As$ terahertz QCLs based on 178 four-quantum-well modules, similar to those in refs 9 and 10. Figure 1a illustrates QCL operation at the designed zero-field operational bias. The laser transition takes place between levels $|6\rangle$ and $|5\rangle$ ($E_{6,5} \approx 13$ meV → 3.1 THz) followed by a fast, LO-phonon assisted relaxation towards the triplet ground states $|3\rangle$, $|2\rangle$ and $|1\rangle$. A magnetic field allows controlled modulation of the lifetime of the laser transition states when the resonance condition is fulfilled ($\varepsilon_{i,0} - \varepsilon_{j,N} - p\hbar\omega_c = 0$), where i is either the upper or lower lasing level, j is a lower sub-band, and p is 0 for elastic scattering and 1 for inelastic scattering. When the upper lasing state is off resonance (quenched non-radiative relaxation) and the lower state is on resonance (enhanced relaxation), population inversion between levels $|6,0\rangle$ and $|5,0\rangle$ increases, thus reducing the lasing threshold current, and increasing laser power and operational temperature.

Electronic structure calculations show that such a resonant enhancement of the $|6,0\rangle \rightarrow |5,0\rangle$ transition (~3 THz), $\varepsilon_{4,0} - \varepsilon_{3,1} = 0$, takes place near 20 T and in a range of voltage biases between ~50 and 70 mV per period (Fig. 1). When the voltage bias is increased above ~60 mV per period, levels $|5,0\rangle$ and $|4,0\rangle$ are separated, but still have a large dipole-matrix element, resulting in the possibility of dual-wavelength 'cascaded' laser transitions: $|6,0\rangle \rightarrow |5,0\rangle$ (~3 THz) followed by $|5,0\rangle \rightarrow |4,0\rangle$ (~1 THz). Further increasing the voltage bias separates levels $|8,0\rangle$, $|7,0\rangle$ and $|6,0\rangle$. At these biases, both $|8,0\rangle \rightarrow |7,0\rangle$ and $|5\rangle \rightarrow |4\rangle$ transitions have large dipole-matrix elements, and can be enhanced by a LL resonance at 31 T (Fig. 1e) and 23 T (see also Supplementary Information, Discussion). Following the model of inhomogeneous LL broadening caused by the macroscopic fluctuations of quantum well parameters[20], a phenomenological Gaussian broadening of the LLs with a width of $\delta = 4$ meV is introduced, which is consistent with previous estimates in mid-infrared and terahertz QCLs of 2–6 meV (refs 16, 19, 20).

The electrical characteristics, current density J, voltage/period V, emitted optical power P as well as emission spectra were

[1]National High Magnetic Field Laboratory, Tallahassee, Florida 32310, USA, [2]Massachusetts Institute of Technology, Department of Electrical Engineering and Computer Science and Research Laboratory of Electronics, Cambridge, Massachusetts 02139, USA, [3]Department of Electrical Engineering and California NanoSystems Institute, University of California, Los Angeles, California 90095, USA, [4]Sandia National Laboratories, Department 1123, MS 0601, Albuquerque, New Mexico 87185-0601, USA; *e-mail: smirnov@magnet.fsu.edu

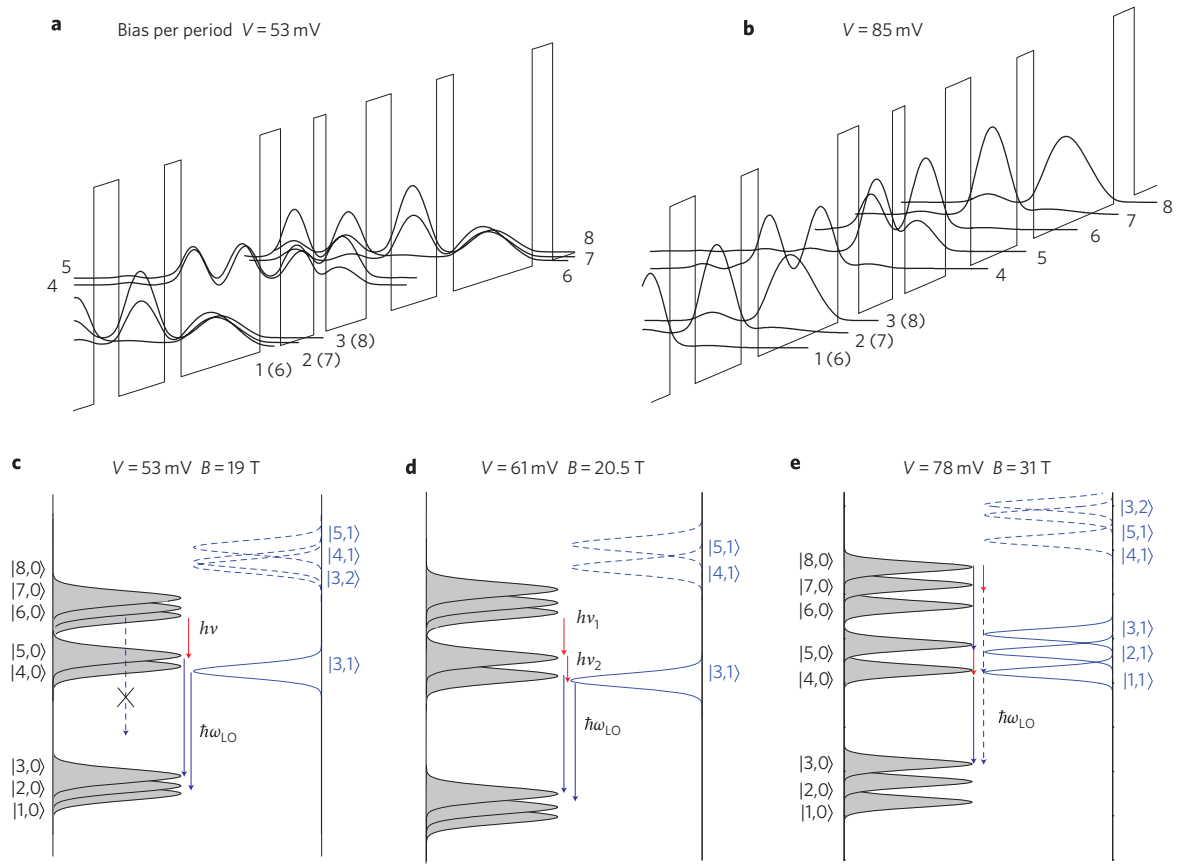

Figure 1 | Calculated electronic structure. a,**b**, Conduction band diagrams and squared wavefunctions of the relevant sub-band states. Levels 3,2,1 are levels 8,7,6 for the next period. At 53 mV per period, zero B-field operational bias, the laser transition takes place from 6 → 5 with fast LO-phonon assisted relaxation (5,4 → 3,2). At higher biases, the closely spaced levels (8,7,6) and (5,4) split, making additional transitions possible. **c**–**e**, The electronic structure in a magnetic field. Illustration (**c**) of the field-induced resonant enhancement of the lasing transition between LLs $|6,0\rangle$ and $|5,0\rangle$ (red arrow). Inelastic scattering by LO-phonon emission from the upper laser transition state is quenched (arrow with an ×), while elastic scattering from the final state $|4,0\rangle$ to another LL ($|3,1\rangle$) is allowed. Cascade lasing process (**d**) at $V^* = 61$ mV, $|6,0\rangle \rightarrow |5,0\rangle$, $|5,0\rangle \rightarrow |4,0\rangle$. Illustration (**e**) of the possible paths for light production in a magnetic field at $V^* = 78$ mV. The inhomogeneous LL broadening is 4 meV. Blue arrows indicate LO-phonon assisted relaxation ($\hbar\omega = 36$ meV).

recorded as a function of the external magnetic field applied perpendicular to the plane of the quantum wells. The optical power was measured using two fast detectors: a Ge:Ga photodetector with a low-frequency cut-off at 2 THz and an InSb hot electron bolometer with a high-frequency limit of 2.4 THz. Laser emission measured with two spectrally selective detectors revealed strong magnetic field dependence, as shown in Fig. 2. The differences in relative intensities for both detectors at $B > 15$ T clearly indicate changes of the emission energy. Sharp changes in the optical power arise with the formation of well-defined plateaus in the voltage curves, indicating three stable voltage alignments (Fig. 2c,d). Plotting the optical power versus the recorded voltage clearly shows these three distinct lasing zones (Fig. 3). Zone 1 emission is observed at biases between 50 and 58 mV/period, with lasing in a single band centred on 3 THz. As J increases, the QCL realigns to zone 2 (59–73 mV per period) with strong sub-terahertz lasing in two fixed main modes, 0.97 and 0.85 THz, in addition to the 3 THz band. Calibrated terahertz optical power measurements in high magnetic fields are difficult to obtain. By comparing the measured terahertz emission power from the same devices at zero field, we estimate the maximum 1 THz power at 20.5 T to be at least 1–2 mW. Further increasing J results in a third zone between 78 and 96 mV, where the 3 THz band disappears and the sub-terahertz lasing blueshifts towards 2 THz. The spectra over the measured J and B (Fig. 4a) show a broad range of lasing, with modes as low as 0.68 THz at 31 T and as high as 3.33 THz at 19 T. The possibility of multi-wavelength lasing is enabled by the metal–metal waveguide, which has low losses and strong modal confinement over the entire terahertz range[18,21]. (See Supplementary Information, Discussion, for a representative set of $P(B,J)$, $V(B,J)$ characteristics and spectra.)

In Fig. 3b, we compare the experimental lasing energies to the calculated energies of the transitions with the highest probability of lasing. This confirms that the 3 THz light is attributed to a $|6\rangle \rightarrow |5\rangle$ transition. For further analysis, we consider possible current paths through the structure when each sub-band breaks into a set of LLs, and compare the LL crossings to the positions of the observed emission minima and maxima (see Supplementary Information, Discussion). This unequivocally confirms that the 3 THz emission in zones 1 and 2 originates from a $|6,0\rangle \rightarrow |5,0\rangle$ transition. In zone 2, population inversion between $|5,0\rangle$ and $|4,0\rangle$ is achieved by the field-induced depopulation of $|4,0\rangle$, and the continued long lifetime of level $|6,0\rangle$. This allows for the observed strong dual-frequency lasing (1 and 3 THz) that originates from the simultaneous emission from two cascaded optical transitions in each period: $|6,0\rangle \rightarrow |5,0\rangle$ and $|5,0\rangle \rightarrow |4,0\rangle$. A $|8,0\rangle \rightarrow |7,0\rangle$ optical transition is excluded because of the strong overlap of the LLs in zone 2. This is the first terahertz dual-frequency cascaded quantum cascade structure. It is also worth noting that a 'cascaded' dual-frequency emission has recently been successfully implemented at MIR frequencies, opening up the possibility of producing correlated photons in quantum cascade structures[22,23].

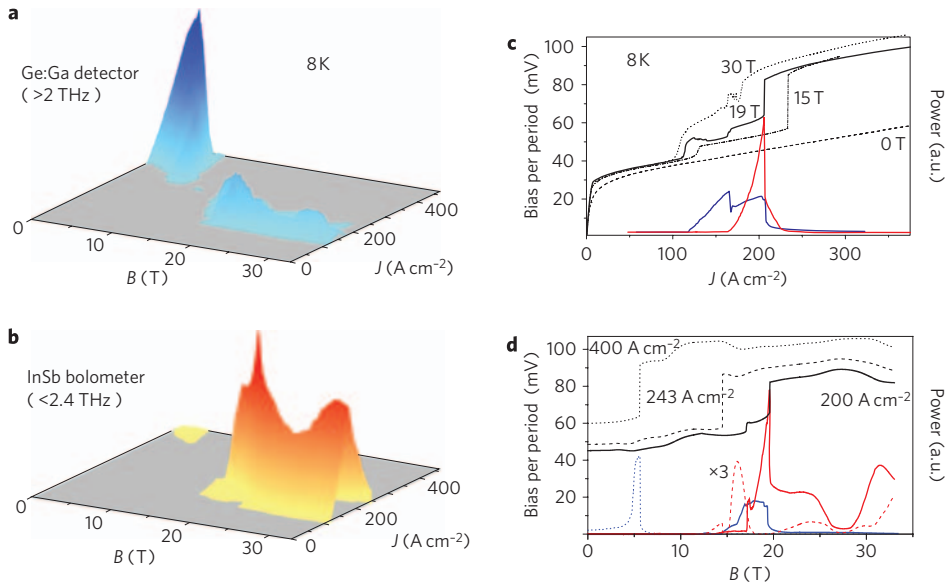

Figure 2 | Optical and electrical characteristics of a terahertz QCL device in a magnetic field. a,**b**, Three-dimensional plot of the optical power *P* versus the magnetic field *B* and current density *J* measured at 8 K, with a Ge:Ga photoconductor (in blue, **a**) and an InSb hot electron bolometer (in red, **b**). **c**, Voltage *V* versus *J* at different magnetic fields (black curves). Data for 19 T are given in solid lines. The blue and red curves depict the optical power measured using the Ge:Ga and InSb detectors, respectively . **d**, *P*(*B*) and *V*(*B*) at three different current densities. The optical power for $J = 243$ A cm^{-2} (dashed line) has been multiplied by 3 for better visibility.

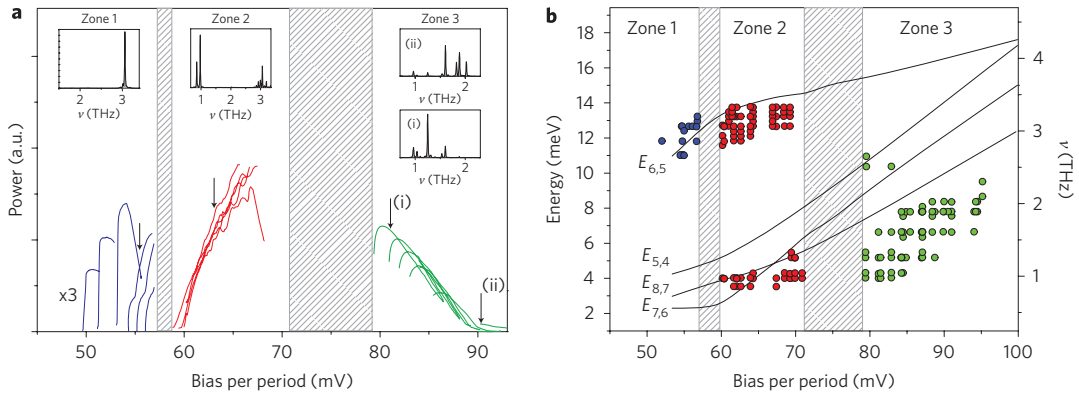

Figure 3 | Laser emission properties as a function of voltage bias. a, Optical power and typical emission spectra measured at 8 K, plotted versus the measured voltage bias, showing three distinct zones of lasing operation separated by unstable bias regions (grey boxes). The *P*(*V*) data was created from *P* and *V* versus *B* at constant *J*. The black arrows indicate the biases for the spectra. **b**, Comparison between the main emission energies from experiment (symbols) and the calculated transition energies for the most probable lasing transitions (lines).

In zone 3, the optical measurements show three maxima at 16 T, 23 T and 31 T (Fig. 2d). Two optical transitions are needed to account for these maxima. Considering that the structure breaks from the traditional resonant tunnelling regime to a Stark-like ladder where $|8\rangle$, $|7\rangle$ and $|6\rangle$ no longer overlap, the peak at 16 T can only be accounted for by a $|8,0\rangle \rightarrow |7,0\rangle$ transition, whereas the brighter light at 23 T and 31 T is dominated by a $|5,0\rangle \rightarrow |4,0\rangle$ transition. In both situations, the lasing transition is helped by elastic scattering and is followed by two LO-phonon assisted relaxations. The difference between the measured and calculated lasing energies is likely due to LL broadening.

Finally, we report QCL performance at high temperatures (Fig. 4b). Lasing continues up to 215 K for 1 THz emission (31 T), and up to 225 K for 3 THz (19.3 T). Fitting the measured threshold temperature dependence to the common phenomenological expression $J_{th} \propto J \exp(T/T_0)$, we obtain values for the figure of merit of $T_0 = (180 \pm 10)$ K for both cases, compared to $T_0 = 130$ K (refs 9 and 10) measured without a magnetic field—a significant improvement[24]. The effect of the magnetic field can be understood from the gain coefficient[25] $g \propto \tau_u(1 - \tau_l/\tau_{ul})z_{ul}^2/\Delta\nu$, where τ_u and τ_l are the upper- and lower-state lasing level lifetimes, τ_{ul} is the non-radiative scattering time, z_{ul} is the optical dipole matrix element, and $\Delta\nu$ is the spontaneous emission linewidth. The main magnetic field contribution arises from an increase of τ_u (quenched non-radiative relaxation) and a decrease of τ_l (resonantly enhanced relaxation). In fact, at $B \approx 20$ T, scattering from the upper radiative state $|6,0\rangle \rightarrow |n,N\rangle$, as well as thermally activated processes, are suppressed for any value of the sub-band n and Landau index N; meanwhile, τ_l decreases, because $\varepsilon_{4,N} - \varepsilon_{3,N} \approx \hbar\omega_c \approx \hbar\omega_{LO}$.

Low-frequency lasing and high-temperature operation are also assisted by a reduction in the homogeneous linewidth, while the inhomogeneous broadening remains large at ~4 meV. This reduction is attributed to the quenching of intra-sub-band dephasing in the magnetic fields[26–28]. The radiative transitions in fact occur between localized micro-states (as opposed to extended plane-wave

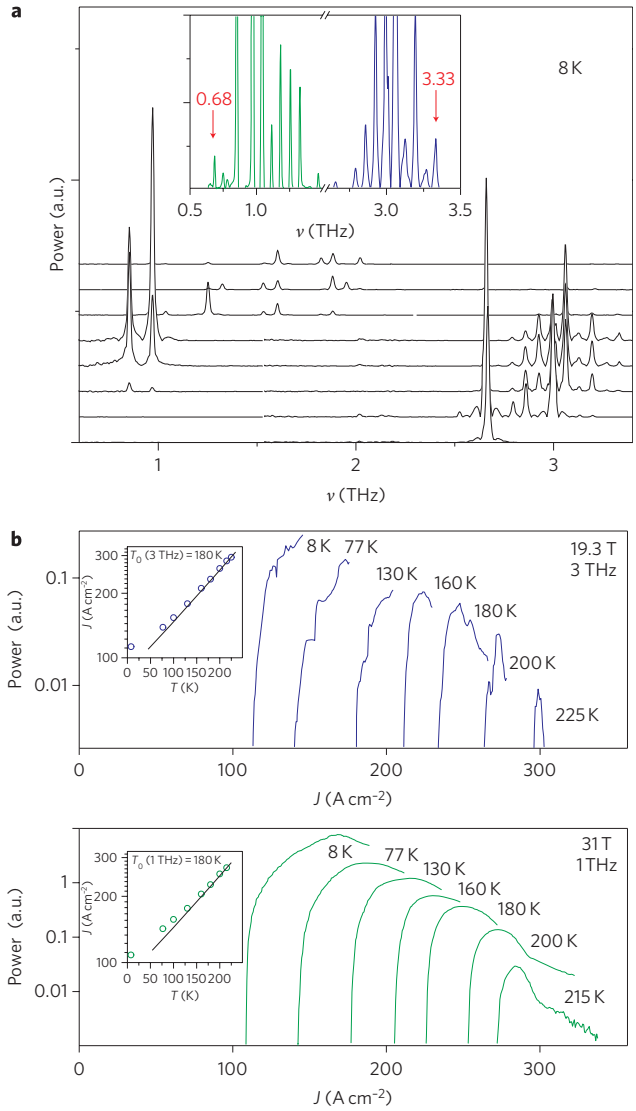

Figure 4 | QCL device performance in terms of spectral coverage and operational temperature. a, Spectral coverage of the QCL device with increasing voltage bias and magnetic field (bottom curve 54.9 mV/period, 13 T; top curve 88.4 mV/period, 25 T). The inset shows the spectral extremes of the QCLs: 0.68 THz (69.9 mV /period, 31.2 T) and 3.33 THz (63.9 mV/period, 19 T). **b**, Temperature dependence of $P(J)$ at two enhanced lasing positions at 19.3 T and 31 T. The insets show the current density threshold as a function of temperature. 1 THz lasing has been omitted from the 19.3 T curves for visual clarity.

states in the absence of magnetic fields), which, because of their sharp energy levels, will be able to maintain a population inversion. The effect of the large inhomogeneous broadening is simply to spread the gain over more frequencies, but as long as the population inversion condition is maintained ($\tau_l < \tau_{ul}$) positive gain is available, even when $\nu < \Delta\nu$.

In conclusion, we report strong, magnetic-field-assisted, multi-wavelength emission in a QCL. By applying appropriate electrical and magnetic fields, we have achieved 3 THz (1 THz) laser emission at temperatures up to 225 K (215 K) at 19.3 T (31 T), or have changed the emission frequency over an unprecedented range (from 0.68 to 3.33 THz). We have therefore demonstrated the longest wavelength, the widest spectral coverage, and the highest operational temperatures in any single terahertz solid-state laser to date. Furthermore, these results bear out the prediction that lateral quantum confinement, provided either magnetically, electrostatically or structurally (that is, a quantum box), is a route to higher temperature operation for terahertz QCLs.

Methods

Devices and measurements. The devices used (labelled FL178C-M7) were $GaAs/Al_{0.15}Ga_{0.85}As$ terahertz QCLs based on 178 four-quantum-well modules processed into metal–metal waveguides, similar to those in refs 9 and 10. Several QCL devices processed into striped ridges 40 to 150 μm wide and from 0.6 to 1.0 mm long were measured mounted in a variable-temperature cryostat inserted in the bore of a resistive magnet capable of producing fields up to 33.4 T such that the magnetic field lines were perpendicular to the plane of the quantum wells and parallel to the direction of the current. Measurements were performed with a current pulser at 14 A cm^{-2} and 1 T steps from 114 to 400 A cm^{-2} and 0 to 33 T. The pulsewidth was ~1–3 μs, with a repetition frequency up to 3 kHz. The light was monitored using two fast terahertz detectors: a spreadfield magnetically enhanced InSb bolometer with a high-frequency limit of 2.4 THz and a Ge:Ga photoconductor with a low-frequency cut-off at 2 THz. Spectra were taken with a Bruker 66 FTIR spectrometer and normalized to the spectral response of the detectors (see Supplementary Information, Discussion).

Received 10 August 2008; accepted 3 December 2008; published online 14 December 2008

References

1. Köhler, R. *et al.* Terahertz semiconductor-heterostructure laser. *Nature* **417,** 156–159 (2002).
2. Walther, C. *et al.* Quantum cascade lasers operating from 1.2 to 1.6 THz. *Appl. Phys. Lett.* **91,** 131122 (2007).
3. Lee, A. *et al.* Real-time terahertz imaging over a standoff distance (>25 meters). *Appl. Phys. Lett.* **89,** 141125 (2006).
4. Faist, J. *et al.* Quantum cascade laser. *Science* **264,** 553–556 (1994).
5. Devenson, J., Teissier, R., Cathabard, O. & Baranova, A. N. InAs/AlSb quantum cascade lasers emitting below 3 μm. *Appl. Phys. Lett.* **90,** 111118 (2007).
6. Colombelli, R. *et al.* Far-infrared surface-plasmon quantum-cascade lasers at 21.5 μm and 24 μm wavelengths. *Appl. Phys. Lett.* **78,** 2620–2622 (2001).
7. Yu, J. S. *et al.* Temperature dependent characteristics of λ ~3.8 μm room-temperature continuous-wave quantum-cascade lasers. *Appl. Phys. Lett.* **88,** 251118 (2006).
8. Williams, B. S. *et al.* 3.4-THz quantum cascade laser based on longitudinal-optical-phonon scattering for depopulation. *Appl. Phys. Lett.* **82,** 1015–1017 (2007).
9. Williams, B. S. *et al.* Operation of terahertz quantum-cascade lasers at 164 K in pulsed mode and at 117 K in continuous-wave mode. *Opt. Express* **13,** 3331–3339 (2005).
10. Belkin, M. A. *et al.* Terahertz quantum cascade lasers with copper metal–metal waveguides operating up to 178 K. *Opt. Express* **16,** 3242–3248 (2008).
11. Wingreen, N. S. & Stafford, C. A. Quantum-dot cascade laser: Proposal for an ultralow-threshold semiconductor laser. *IEEE J. Quantum Electron.* **33,** 1170–1173 (1997).
12. Hsu, C. F., O, J. S., Zory, P. & Botez, D. Intersubband quantum-box semiconductor lasers. *IEEE J. Sel. Top. Quantum Electron.* **6,** 491–503 (2000).
13. Kastalsky, A. *et al.* Magnetic field-induced suppression of acoustic phonon emission in a superlattice. *J. Appl. Phys.* **69,** 841–845 (1991).
14. Blank, A. *et al.* Suppression of intersubband nonradiative transitions by a magnetic field in quantum well laser devices. *J. Appl. Phys.* **74,** 4795–4796 (1993).
15. Smirnov, D. *et al.* Control of electron-optical-phonon scattering rates in quantum box cascade lasers. *Phys. Rev. B* **66,** 121305(R) (2002).
16. Leuliet, A. *et al.* Electron scattering spectroscopy by a high magnetic field in quantum cascade lasers. *Phys. Rev. B* **73,** 085311 (2006).
17. Alton, J. *et al.* Magnetic field in-plane quantization and tuning of population inversion in a THz superlattice quantum cascade laser. *Phys. Rev. B* **68,** 081303(R) (2003).
18. Scalari, G. *et al.* Terahertz emission from quantum cascade lasers in the quantum Hall regime: Evidence for many body resonances and localization effects. *Phys. Rev. Lett.* **93,** 237403 (2004).
19. Pere-Laperne, N. *et al.* Inter-Landau level scattering and LO-phonon emission in terahertz quantum cascade laser. *Appl. Phys. Lett.* **91,** 062102 (2007).
20. Becker, C. *et al.* Electron-longitudinal optical phonon interaction between Landau levels in semiconductor heterostructures. *Phys. Rev. B* **69,** 115328 (2004).
21. Kohen, S. *et al.* Electromagnetic modeling of terahertz quantum cascade laser waveguides and resonators. *J. Appl. Phys.* **97,** 053106 (2005).
22. Sirtori, C. *et al.* Dual-wavelength emission from optically cascaded intersubband transitions. *Opt. Lett.* **23,** 463–465 (1998).
23. Franz, I. *et al.* Evidence of cascaded emission in a dual-wavelength quantum cascade laser. *Appl. Phys. Lett.* **90,** 091104 (2007).
24. Williams, B. S. Terahertz quantum-cascade lasers. *Nature Photon.* **1,** 517–525 (2007).

25. Gmachl, C. *et al*. Recent progress in quantum cascade lasers and applications. *Rep. Progr. Phys.* **64,** 1533–1601 (2001).
26. Ulrich, J. *et al*. Magnetic-field-enhanced quantum-cascade emission. *Appl. Phys. Lett.* **76,** 19–21 (2000).
27. Blaser, S. *et al*. Terahertz intersubband emission in strong magnetic fields. *Appl. Phys. Lett.* **81,** 67–69 (2002).
28. Scalari G. *et al*. THz and sub-THz quantum cascade lasers. *Laser Photon. Rev.*, accepted for publication, DOI: 10.1002/lpor.200810030, 1–22 (2008).

Acknowledgements

The measurements were performed at the National High Magnetic Field Laboratory supported by the National Science Foundation Cooperative Agreement No. DMR-0084173, by the State of Florida, and by the Department of Energy. The work at Massachusetts Institute of Technology is supported by Air Force Office of Scientific Research, National Aeronautics and Space Administration, and National Science Foundation. Sandia is a multiprogram laboratory operated by Sandia Corporation, a Lockheed Martin Company, for the United States Department of Energy under Contract DE-AC04-94AL85000.

Additional information

Supplementary Information accompanies this paper at www.nature.com/naturephotonics. Reprints and permission information is available online at http://npg.nature.com/reprintsandpermissions/. Correspondence and requests for materials should be addressed to D.S.